FINITE VOLUME THEORY APPLIED TO TOPOLOGY OPTIMIZATION OF CONTINUUM LINEAR ELASTIC STRUCTURES

Marcelo Vitor Oliveira Araujo

Eduardo Nobre Lages

Márcio André Araújo Cavalcante

marcelo.vitor.o.a@gmail.com

enl@lccv.ufal.br

marcio.cavalcante@ctec.ufal.br

Federal University of Alagoas

Av. Lourival Melo Mota, Tabuleiro do Martins, CEP: 57072-900, Maceió, Alagoas, Brasil.

Abstract. *Numerical stability is an important issue for the gradient-based optimization algorithms based on finite-element method, and is currently one of the main research areas. Numerical issues of the gradient-based optimization algorithms are checkerboards, mesh dependence and local optima. Possible solutions for the checkerboard-problem and mesh dependence are the adoption of higher order elements or filtering techniques based on image processing. The issues of the gradient-based optimization algorithms are mainly related to the displacement based finite-element method assumptions, as the satisfaction of equilibrium and compatibility conditions between elements are enforced only at the nodes, in terms of nodal displacements and forces. Also, the equilibrium equations are not satisfied at the element level, only when a sufficiently refined mesh is employed. Differently of the finite element method, the finite volume theory satisfies the equilibrium equations at the subvolume level, and also the equilibrium and compatibility conditions at the subvolumes' interfaces, in terms of displacements and tractions. The finite volume theory is an elasticity-based approach, so, the connections between subvolumes occur through the subvolumes' faces, as expected from a continuum mechanics point-of-view, which is not true for the displacement based finite-element approach, where the connections between elements occur through the nodes, sometimes resulting in unrealistic optimized geometries with checkerboard patterns, not suitable for manufacturing. A topology optimization approach based on the finite volume theory is proposed to solve these issues of the gradient-based topology optimization algorithms based on finite-element analysis, resulting in an efficient computational tool for topological optimization of continuum linear elastic structures.*

Keywords: *Finite volume theory; Finite Element Method; Gradient-based Optimization Algorithm; Topology Optimization; Continuum Linear Elastic Structures.*

Proceedings of the XXXVIII Iberian Latin-American Congress on Computational Methods in Engineering P.O. Faria, R.H. Lopez, L.F.F. Miguel, W.J.S. Gomes, M. Noronha (Editores), ABMEC, Florianópolis, SC, Brazil, November 5-8, 2017.

1 INTRODUCTION

The continuously increasing computational power has stimulated the use of optimization techniques on the design of materials and structural components. Initially employed by the aeronautic industry, aiming high performance and cost savings, optimized designs have been used by other industries (automobile, oil, electronics, etc.). The topology optimization can find or suggest solutions not initially apparent to engineers. First introduced by Bendsøe and Kikuchi (1988), topology optimization is a powerful optimization technique, and aimed to find the optimal solutions for the given loads, boundary conditions and specified design responses, while the traditional design approach is time consuming and usually leads to ineffective designs.

Within a given design domain, the topology optimization seeks for the best use of material, finding the optimal load path for a specific load and boundary conditions. The topology optimization can be classified by the number of objectives, for one objective the process is known as a Single Objective Analysis (SOA), and for more than one objective the process is referred to as a Multi-Disciplinary Optimization (MDO) or a Multi-Objective Analysis (MOA). Considering the different types of domains, the topology optimization can also be divided into treatment of continuum and discrete structures.

The topology optimization is usually based on finite-element analysis of a discretized domain, thus, in order to obtain reasonable results, the number of finite-elements must be high, once the optimized geometry is a direct result of the mesh size, as only whole elements can be removed or altered, Bendsøe and Sigmund (2004). The resulting optimized geometry obtained from a finite-element analysis is non-smooth, so, a smoothing procedure must be performed once many engineering applications require smooth geometries suitable for manufacturing.

Topology optimization can be defined for continuum structures as a material distribution problem, where the goal is to find the best material distribution in a design domain. Most of the employed optimization algorithms search for a minimum compliance design, which means to maximize the stiffness, and, for this purpose, they have the strain energy as an objective function that must be minimized for a given volume fraction of the design space. Once the topology optimization is based on finite-element analysis, the problem has a design variable for each finite-element, usually a relative material density ρ_e associated with the element e, Bendsøe and Sigmund (2004). The elastic modulus E_e is assumed constant in the element and proportional to the relative material density ρ_e, thus, varying the relative material density will influence the stiffness of the element and also the total material distribution. A Black/White-model is defined as having 0 or 1 values for the relative material density, however, the density is treated as a continuous variable, and the difference between topology algorithms is how they handle intermediate density values. In this sense, the topology theory can be separated between gradient-based and non-gradient-based algorithms, or a combination of both approaches.

A gradient-based model to topology optimization is the so-called “power-law approach” or SIMP approach (Solid Isotropic Material with Penalization), Bendsøe (1989), Zhou and Rozvany (1991), and Mlejnek (1992). The elastic modulus E_e at the element e is evaluated as the relative material density ρ_e raised to some power p times the initial or referential elastic modulus E_e^0, $E_e = (\rho_e)^p E_e^0$. Assuming $p > 1$ makes intermediate values for the relative material density unfavorable, once the stiffness/volume ratio will decrease. Values of $p > 3$ is assumed to perform well for both 2D and 3D analysis, Eschenauer and Olhoff (2001). The

power-law approach usually starts with a uniform distribution of the relative material densities in the elements of the discretized design domain and a specified volume fraction. The first step in the iterative procedure is a finite-element analysis of the boundary value problem, followed by a sensitive analysis based on the derivatives of the design variables. For numerical stability, filtering techniques are employed before updating the densities using the minimum compliance criteria. This procedure is repeated until convergence is achieved.

Numerical stability is an important issue for the gradient-based optimization algorithms, and is currently one of the main research areas. For instance, adopting a lower bound to the relative material densities $\rho_{min} \leq \rho_e \leq 1$ can prevent singularities in the finite-element analysis.

Other numerical issues of the gradient-based optimization algorithms are checkerboards, mesh dependence and local minima. Initially, the checker-boarding was interpreted as some sort of optimal microstructure, but is actually a result of bad numerical modeling. Possible solutions for the checkerboard-problem are the adoption of higher order elements or filtering techniques based on image processing. In the image filter, the design variable sensitivity of the elements are dependent on the weighted average of their respective neighboring elements. Both approaches are computationally expensive, but they are necessary to obtain robust results. These procedures can also help to solve the mesh dependence problem, as suggested by Sigmund and Petersson (1998). The mesh dependence problem is also related with the local minima issue. As well known, the gradient-based algorithms can present problems to find a global minima, once small changes in the simulation parameters can result in a local minima instead of a global minima solution. Different procedures have been suggested to solve this problem, for instance, the continuation scheme, where a gradually increase of the density penalty factor p is employed during the process, which ensures the convexity of the process, avoiding a local minima and gradually converging to the desired 0-1 design, Petersson and Sigmund (1998) and Stolpe and Svanberg (2001a,b).

Other gradient-based algorithms for topology optimization are the Rational Approximations of Material Properties (RAMP)-model and the Homogenization Based Optimization (HBO). Non-gradient-based algorithms include the simulated biological growth (SBG), particle swarm optimization (PSO), evolutionary structural optimization (ESO), bidirectional ESO (BESO) and metamorphic development (MD), Rouhi (2009). The non-gradient-based algorithms are based on binary design variables (solid-void) and problems with *grey* areas (intermediate values) is not an issue.

The finite volume theory has been shown to be a well-suited method for the elastic stress analysis in solid mechanics. Comparison of results generated using this theory with analytical solutions and finite element method results has provided rigorous verifications of this approach, Cavalcante et al. (2007a, 2007b, 2008), and Cavalcante and Pindera (2012a,b). The satisfaction of equilibrium equations at the subvolume level and the concomitant displacement and traction continuities enforced in an average-sense between common faces of distinct subvolumes reveal the strength of this approach, providing a stable and suitable theory for elastic stress analysis in solid mechanics, Cavalcante and Pindera (2012a,b).

The issues of the gradient-based optimization algorithms, especially the checkerboard pattern, are mainly related to the displacement based finite-element method assumptions, as the satisfaction of equilibrium and compatibility conditions between elements enforced only at the nodes, in terms of nodal displacements and forces. Also, the equilibrium equations are not

satisfied at the element level, only when a sufficiently refined mesh is employed. Differently, the finite volume theory satisfies the equilibrium equations at the subvolume level, and also the equilibrium and compatibility conditions at the subvolumes' interfaces, in terms of displacements and tractions. The finite volume theory is an elasticity-based approach, so, the connections between subvolumes occur through the subvolumes' faces, as expected from a continuum mechanics point-of-view, which is not true for the displacement based finite-element approach, where the connections between elements occur through the nodes, sometimes resulting in unrealistic optimized geometries with checkerboard patterns, not suitable for manufacturing.

With the main motivation to solve these issues of the gradient-based topology optimization algorithms based on finite-element analysis, it is proposed a topology optimization approach based on the finite volume theory. The structural topology optimization based on the power-law approach and the finite volume theory have not shown the checkerboard pattern for different types of boundary conditions and geometries, even when no filters are employed, differently of the same approach using the displacement based finite-element method, where the checkerboard pattern exists for the Q4-element in the absence of filters.

Comparison of the results obtained by the topology optimization procedure based on finite volume theory with those ones obtained by the same approach based on finite-element analysis provides a good understanding of the advantages and limitations of the proposed technique. Also, a good investigation has been conducted about the numerical stability of the proposed approach, i.e., if some numerical issues of the finite-element based approach occur at the proposed technique, as the checkerboards, mesh dependence and local minima.

2 THEORY OF LINEAR ELASTICITY

Consider an elastic solid of volume V, delimited by a surface S and subjected to the action of body forces $\mathbf{b} = b_2\hat{\mathbf{e}}_2 + b_3\hat{\mathbf{e}}_3$ and superficial forces $\mathbf{t} = t_2\hat{\mathbf{e}}_2 + t_3\hat{\mathbf{e}}_3$. In order to perform a two-dimensional analysis in the plane $x_2 - x_3$, in which a regime of small displacements and strains is considered, the definition of the engineering strain tensor is given by:

$$\boldsymbol{\varepsilon} = \frac{1}{2}\left[\nabla\mathbf{u} + (\nabla\mathbf{u})^T\right] \text{ (strain-displacement relationship)} \tag{1}$$

where $\boldsymbol{\varepsilon} = \begin{bmatrix} \varepsilon_{22} & \varepsilon_{23} \\ \varepsilon_{32} & \varepsilon_{33} \end{bmatrix}$, $\nabla = \hat{\mathbf{e}}_2\frac{\partial}{\partial x_2} + \hat{\mathbf{e}}_3\frac{\partial}{\partial x_3}$ and $\mathbf{u} = u_2\hat{\mathbf{e}}_2 + u_3\hat{\mathbf{e}}_3$ represent the engineering strain tensor, the gradient operator and the displacement field, respectively.

Once the strain components are known, the stress components can be determined by the Generalized Hooke's Law, shown below:

$$\sigma_{ij} = C_{ijkl}\varepsilon_{kl} \text{ (material constitutive relationship)} \tag{2}$$

where σ_{ij} and ε_{ij} are the stress and strain tensors at any point on the solid, in this order, and C_{ijkl} is the material constitutive tensor. In addition, in the case of a stress analysis, the following integral form of the equilibrium equations is available:

$$\int_S \mathbf{t}dS + \int_V \mathbf{b}dV = \int_V (\nabla\boldsymbol{\sigma} + \mathbf{b})dV = \mathbf{0} \quad \text{(equilibrium equations)} \tag{3}$$

3 FINITE VOLUME THEORY

Figure 1 shows a rectangular structure subdivided in $N_q = N_\beta N_\gamma$ rectangular subdomains called subvolumes. The values N_β and N_γ indicate the number of subdivisions corresponding to the intervals $0 \le x_2 \le B$ and $0 \le x_3 \le H$, respectively. Each subvolume can be denoted by a single index q $(1 \le q \le N_q)$ or by a pair of indexes $\beta = 1, \cdots, N_\beta$ and $\gamma = 1, \cdots, N_\gamma$, where q can be evaluated from β and γ. The subvolume (β, γ) occupies the position β in the horizontal direction and the position γ in the vertical direction, or $q = \gamma + (\beta - 1)N_\gamma$ for the discretized structure. Furthermore, the stresses and displacements imposed on the structure are applied to the external faces of the subvolumes located on the boundaries of the structural model, in terms of average values of the static and kinematic quantities.

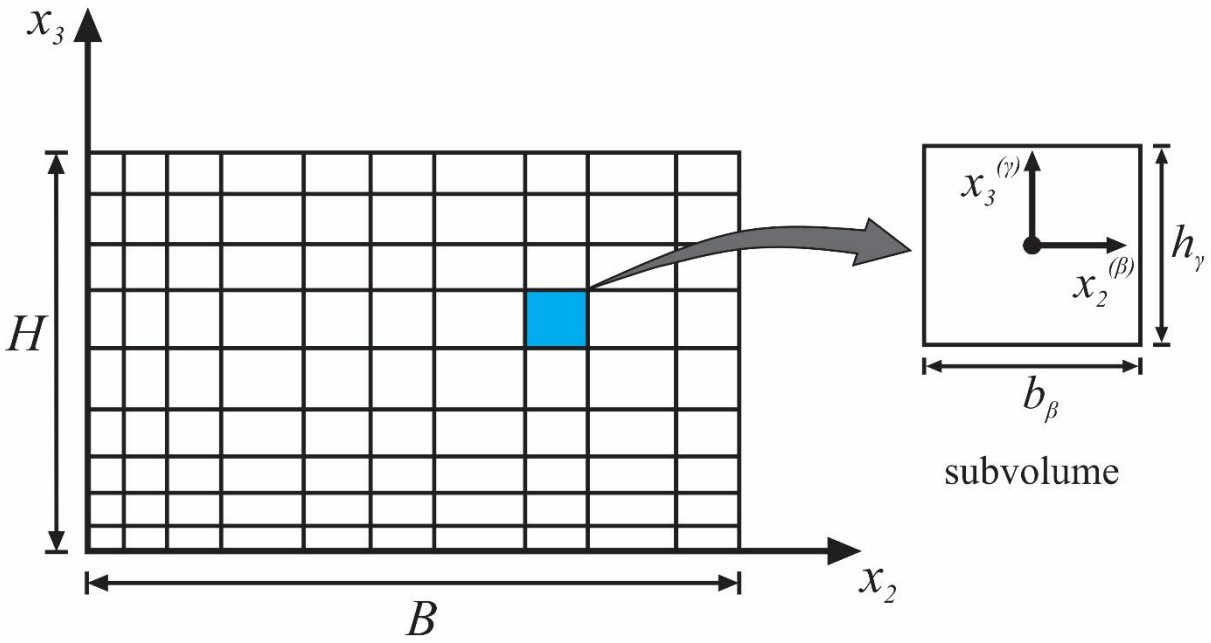

Figure 1. Discretized structure in rectangular subvolumes and local coordinate system of a generic subvolume.

The present formulation employs second-degree polynomials expressed as a function of local coordinates to approximate the components of the displacement field in each subvolume, making possible the stress analysis of solids (Bansal and Pindera, 2003). These polynomials are given by:

$$u_i^{(q)} = U_{i(00)}^{(q)} + x_2^{(q)} U_{i(10)}^{(q)} + x_3^{(q)} U_{i(01)}^{(q)} + \frac{1}{2}\left(3\left(x_2^{(q)}\right)^2 - \frac{b_q^2}{4}\right) U_{i(20)}^{(q)} + \frac{1}{2}\left(3\left(x_3^{(q)}\right)^2 - \frac{h_q^2}{4}\right) U_{i(02)}^{(q)} \tag{4}$$

in which $b_q\left(=b_\beta\right)$ and $h_q\left(=h_\gamma\right)$ represent the width and height of a generic subvolume, and the values $U_{i(mn)}^{(q)}$ are the unknown coefficients of the displacement field.

3.1 Local Stiffness Matrix

In the present formulation, it is necessary to calculate the surface-averaged values of the displacement field components. For this, the following equations are employed:

$$\bar{u}_i^{(q,p)} = \frac{1}{b_q}\int_{-b_q/2}^{+b_q/2} u_i^{(q)}\left(x_2^{(q)}, \mp h_q/2\right) dx_2^{(q)} \text{ , for } p=1, 3 \tag{5}$$

$$\bar{u}_i^{(q,p)} = \frac{1}{h_q}\int_{-h_q/2}^{+h_q/2} u_i^{(q)}\left(\pm b_q/2, x_3^{(q)}\right) dx_3^{(q)} \text{ , for } p=2, 4 \tag{6}$$

where $\bar{u}_i^{(q,p)}$ are the surface-averaged displacements of a generic subvolume q.

Using the components of the displacement field, Eq. (4), in the two equations above, eight expressions are obtained for the surface-averaged displacements as a function of the displacement field coefficients. Such expressions can be organized in matrix notation as follows:

$$\bar{\mathbf{u}}^{(q)} = \mathbf{A}_{(8\times 8)}^{(q)}\mathbf{U}^{(q)} + \mathbf{a}_{(8\times 2)}^{(q)}\mathbf{U}_{(00)}^{(q)} \tag{7}$$

where $\bar{\mathbf{u}}^{(q)} = \left[\bar{u}_2^{(q,1)}, \bar{u}_3^{(q,1)}, \bar{u}_2^{(q,2)}, \bar{u}_3^{(q,2)}, \bar{u}_2^{(q,3)}, \bar{u}_3^{(q,3)}, \bar{u}_2^{(q,4)}, \bar{u}_3^{(q,4)}\right]^T$ is the surface-averaged displacement vector, $\mathbf{U}^{(q)} = \left[U_{2(10)}^{(q)}, U_{2(01)}^{(q)}, U_{2(20)}^{(q)}, U_{2(02)}^{(q)}, \ldots, U_{3(02)}^{(q)}\right]^T$ is the vector with the coefficients of first and second order and $\mathbf{U}_{(00)}^{(q)} = \left[U_{2(00)}^{(q)}, U_{2(00)}^{(q)}\right]^T$ is the vector with the coefficients of zero order. The vector with the coefficients of first and second order can be evaluated as a function of the surface-averaged displacement vector and the vector with the coefficients of zero order as follows:

$$\mathbf{U}^{(q)} = \left(\mathbf{A}_{(8\times 8)}^{(q)}\right)^{-1}\bar{\mathbf{u}}^{(q)} - \left(\mathbf{A}_{(8\times 8)}^{(q)}\right)^{-1}\mathbf{a}_{(8\times 2)}^{(q)}\mathbf{U}_{(00)}^{(q)} \tag{8}$$

By replacing the components of the displacement field in Eqs. (1) and (2), the local components of the strain and stress fields are obtained for a generic subvolume q as a function of the displacement field coefficients. In order to evaluate the components of the stress tensor, the subvolume material was considered to be linear elastic, isotropic and homogeneous. With the stress tensor, we can determine the components of the traction vectors acting on the faces of a generic subvolume, as shown below:

$$t_i^{(q,p)}\left(x_2^{(q)}\right) = \mp\sigma_{3i}^{(q)}\left(x_2^{(q)}, \mp h_q/2\right) \text{ (for } p=1, 3) \tag{9}$$

$$t_i^{(q,p)}\left(x_3^{(q)}\right) = \pm\sigma_{2i}^{(q)}\left(\pm b_q/2, x_3^{(q)}\right) \text{ (for } p=2, 4) \tag{10}$$

Evaluating Equations (9) and (10) in a surface-averaged sense for a generic subvolume, using definitions similar to those shown in Eqs. (5) and (6), eight expressions are found, which can be organized in matrix notation as follows:

$$\bar{\mathbf{t}}^{(q)} = \mathbf{B}_{(8\times8)}^{(q)} \mathbf{U}^{(q)} \tag{11}$$

where $\bar{\mathbf{t}}^{(q)} = \left[\bar{t}_2^{(q,1)}, \bar{t}_3^{(q,1)}, \bar{t}_2^{(q,2)}, \bar{t}_3^{(q,2)}, \bar{t}_2^{(q,3)}, \bar{t}_3^{(q,3)}, \bar{t}_2^{(q,4)}, \bar{t}_3^{(q,4)}\right]^T$ is the surface-averaged traction vector for a generic subvolume q.

The surface-averaged traction vector acting in each face of a generic subvolume can be expressed in matrix notation as follows:

$$\bar{\mathbf{t}}^{(q,p)} = \mathbf{B}_{(2\times8)}^{(q,p)} \left(\mathbf{A}_{(8\times8)}^{(q)}\right)^{-1} \bar{\mathbf{u}}^{(q)} - \mathbf{B}_{(2\times8)}^{(q,p)} \left(\mathbf{A}_{(8\times8)}^{(q)}\right)^{-1} \mathbf{a}_{(8\times2)}^{(q)} \mathbf{U}_{(00)}^{(q)} \tag{12}$$

In the absence of body forces, the satisfaction of the equilibrium conditions is ensured by making the sum of the surface forces acting on the subvolume equal to zero, as shown in the following equation:

$$\int_{S_q} \mathbf{t}^{(q)} dS_q = \mathbf{0}_{(2\times1)} \tag{13}$$

In this formulation, the equilibrium equation of a generic subvolume (Equation 13) can be expressed in terms of the surface-averaged traction vectors. Thus, the equation above becomes:

$$\sum_{p=1}^{4} \bar{\mathbf{t}}^{(q,p)} L_p^{(q)} = \mathbf{0}_{(2\times1)} \tag{14}$$

where $L_1^{(q)} = b_q$, $L_2^{(q)} = h_q$, $L_3^{(q)} = b_q$ and $L_4^{(q)} = h_q$ are the lengths of the faces of a generic subvolume.

Using the surface-averaged traction vectors (Equation 12) in the local equilibrium equation of a subvolume (Equation 14), we arrive at the following equation:

$$\left(\sum_{p=1}^{4} \mathbf{B}_{(2\times8)}^{(q,p)} L_p^{(q)}\right) \left(\mathbf{A}_{(8\times8)}^{(q)}\right)^{-1} \bar{\mathbf{u}}^{(q)} - \left(\sum_{p=1}^{4} \mathbf{B}_{(2\times8)}^{(q,p)} L_p^{(q)}\right) \left(\mathbf{A}_{(8\times8)}^{(q)}\right)^{-1} \mathbf{a}_{(8\times2)}^{(q)} \mathbf{U}_{(00)}^{(q)} = \mathbf{0}_{(2\times1)} \tag{15}$$

By isolating the vector with the coefficients of zero order in the Equation 15, we can express this vector as a function of the local surface-averaged displacement vector. The matrices employed in the above equations contain information related to the geometric dimensions and the mechanical properties of the subvolume. The matrix relationship between the vector with the coefficients of zero order and the surface-averaged displacement vector can be defined as follows:

$$\mathbf{U}_{(00)}^{(q)} = \bar{\mathbf{a}}_{(2\times8)}^{(q)} \bar{\mathbf{u}}^{(q)} \tag{16}$$

where $\bar{\mathbf{a}}_{(2\times8)}^{(q)} = \left(\left(\sum_{p=1}^{4} \mathbf{B}_{(2\times8)}^{(q,p)} L_p^{(q)}\right) \left(\mathbf{A}_{(8\times8)}^{(q)}\right)^{-1} \mathbf{a}_{(8\times2)}^{(q)}\right)^{-1} \left(\sum_{p=1}^{4} \mathbf{B}_{(2\times8)}^{(q,p)} L_p^{(q)}\right) \left(\mathbf{A}_{(8\times8)}^{(q)}\right)^{-1}$. By replacing Eq. (16) in Eq. (8), we can find a matrix relationship between the vector with the first and second order

coefficients of the displacement field with the local surface-averaged displacement vector, resulting in:

$$\mathbf{U}^{(q)} = \overline{\mathbf{A}}_{(8\times 8)}^{(q)} \overline{\mathbf{u}}^{(q)} \tag{17}$$

where $\overline{\mathbf{A}}_{(8\times 8)}^{(q)} = \left(\mathbf{A}_{(8\times 8)}^{(q)}\right)^{-1} - \left(\mathbf{A}_{(8\times 8)}^{(q)}\right)^{-1} \mathbf{a}_{(8\times 2)}^{(q)} \overline{\mathbf{a}}_{(2\times 8)}^{(q)}$. Finally, replacing Eqs. (16) and (17) in Eq. (11), we obtain the local system of equations of a generic subvolume as follows:

$$\bar{\mathbf{t}}^{(q)} = \mathbf{K}_{(8\times 8)}^{(q)} \overline{\mathbf{u}}^{(q)} \tag{18}$$

where $\mathbf{K}_{(8\times 8)}^{(q)} = \mathbf{B}_{(8\times 8)}^{(q)} \overline{\mathbf{A}}_{(8\times 8)}^{(q)}$ is the local stiffness matrix of a generic subvolume q.

3.2 Global Stiffness Matrix Assemblage

The global stiffness matrix of the structure is assembled considering the individual contribution of each subvolume of the discretized domain. If the structure is subdivided in N_q subvolumes, considering two degrees of freedom per face, we have $ndof = 2N_\beta(N_\gamma + 1) + 2(N_\beta + 1)N_\gamma$ degrees of freedom for the structure. Based on the kinematic and static compatibility conditions, which are satisfied in average sense at the interfaces between subvolumes, we arrive at the following equation:

$$\mathbf{T} = \mathbf{K}_{(ndof,ndof)} \mathbf{U} \tag{19}$$

where $\mathbf{U} = \left[\bar{u}_1, \cdots, \bar{u}_{ndof}\right]^T$ and $\mathbf{T} = \left[\bar{t}_1, \cdots, \bar{t}_{ndof}\right]^T$ are the global surface-averaged displacement vector and the global surface-averaged traction vector of the discretized structure, respectively. Based on the compatibility conditions mentioned above, the global stiffness matrix of the structure can be evaluated as follows:

$$\mathbf{K}_{(ndof,ndof)} = \sum_{q=1}^{N_q} \left(\mathbf{L}_{(8\times ndof)}^{(q)}\right)^T \mathbf{K}_{(8\times 8)}^{(q)} \mathbf{L}_{(8\times ndof)}^{(q)} \tag{20}$$

where $\mathbf{L}_{(8\times ndof)}^{(q)}$ and $\left(\mathbf{L}_{(8\times ndof)}^{(q)}\right)^T$ are the kinematic and static compatibility matrices of the structure, respectively.

3.3 Solution of the Global System of Equations

The global system of equations of the structure can be written in the form shown below, after considering the boundary conditions for the global surface-averaged displacement and traction vectors of the discretized structure:

$$\begin{Bmatrix} \mathbf{T}_c \\ \mathbf{T}_d \end{Bmatrix} = \begin{bmatrix} \mathbf{K}_{cd} & \mathbf{K}_{cc} \\ \mathbf{K}_{dd} & \mathbf{K}_{dc} \end{bmatrix} \begin{Bmatrix} \mathbf{U}_d \\ \mathbf{U}_c \end{Bmatrix} \tag{21}$$

where $\mathbf{T}_c$ and $\mathbf{T}_d$ denote the known and unknown surface-averaged traction vectors, respectively, and $\mathbf{U}_c$ and $\mathbf{U}_d$ represent the known and unknown surface-averaged

displacement vectors, respectively. Thus, the unknown surface-averaged displacement and traction vectors can be evaluated by the following equations:

$$\mathbf{U}_d = \left(\mathbf{K}_{cd}\right)^{-1}\mathbf{T}_c - \left(\mathbf{K}_{cd}\right)^{-1}\mathbf{K}_{cc}\mathbf{U}_c \tag{22}$$

$$\mathbf{T}_d = \mathbf{K}_{dd}\mathbf{U}_d - \mathbf{K}_{dc}\mathbf{U}_c \tag{23}$$

4 TOPOLOGY OPTIMIZATION PROBLEM

A topology optimization problem consists of finding a better distribution of the material in a specific domain. The optimum distribution can be encountered by searching which points of the domain will be filled out by isotropic material. However, some numerical instabilities have appeared when we apply this method, such as mesh-dependency, checkerboard pattern, and local minima (Sigmund & Petersson, 1998). Those difficulties have, in circumstances, avoided the application of topology optimization method in industry.

Firstly, the problem of mesh-dependency appears in the case that finer meshes tend to result in a clearer topology. However, in some cases, when we use finer meshes, the results tend to produce complex structures with finer topology, which is different from the resultant model of coarse mesh. Second, in the checkerboard problem, there is an alternation between empty and filled elements, being similar to a checkerboard. Finally, the third instability is related to the fact that the majority of topology optimization problems are non-convex, so there are several local minimums. In this case, the nonconvexity problem can produce different solutions for the same discretized problem (Coutinho, 2006).

According to Sigmund and Petersson (1998), there are possible cures for some instability issues discussed. Table 1 presents and summarizes the cause and possible prevention techniques by Sigmund and Petersson (1998). However, the purpose of this paper is to apply the Finite Volumes Theory (FVT) instead of the Finite Elements Method (FEM) to get better results by avoiding some numerical instabilities, such as those related to checkerboard pattern.

The topology optimization problem, where the major objective is to minimize compliance, can be written as

$$\begin{cases} \min\limits_{\boldsymbol{\rho}} c(\boldsymbol{\rho}) = \boldsymbol{U}^T \cdot \boldsymbol{K} \cdot \boldsymbol{U} = \sum\limits_{e=1}^{N} (\rho_e)^p \cdot \boldsymbol{u_e^T} \cdot \boldsymbol{k_e^0} \cdot \boldsymbol{u_e} \\ \text{subject to:} \quad \dfrac{V(\boldsymbol{\rho})}{\bar{V}} = f \\ \qquad\qquad \boldsymbol{K} \cdot \boldsymbol{U} = \boldsymbol{F} \\ \qquad\qquad \mathbf{0} < \boldsymbol{\rho}_{min} \leq \boldsymbol{\rho} \leq \mathbf{1} \end{cases} \tag{24}$$

where $\boldsymbol{U}$ and $\boldsymbol{F}$ are the global displacement and force vectors, respectively, $\boldsymbol{K}(\boldsymbol{\rho})$ is the global stiffness matrix, $\boldsymbol{u_e}$ and $\boldsymbol{k_e^0}$ are the element displacement vector and stiffness matrix, respectively, $\boldsymbol{\rho}$ is the vector of design variables, $\boldsymbol{\rho}_{min}$ is a vector of minimum relative densities (non-zero to avoid singularity), N is the total number of elements used to discretize the domain, p is the penalization power, $V(\boldsymbol{\rho})$ and $\bar{V}$ are the material volume and design domain volume, respectively, and f is the prescribed volume fraction.

Table 1. Definition of problems found in discretized topology optimization.

Numerical Experience	Mathematical problem	Physical explanation	Prevention techniques
Checkerboards	Nonconvergence of FE-solutions	Erroneous FE-modeling of checkerboards	Higher order finite elements Patches Filtering Restriction methods below
Mesh dependence			
Necessarily finer and finer structure	Nonexistence	"convergence" to microstructure	Relaxation Perimeter Global/local gradient constraint Mesh-independent filtering
Possibly finer and finer structure	Nonuniqueness	Ex.: uniaxial stress	Nothing (maybe manufacturing preferences)
Local minima	Nonconvergence of algorithm	Nonconvexity Flatness	Continuation methods

The problem presented in Eq. (24) can be solved by a variety of different methods. However, this article applied the Optimality Criteria (OC) method due to its simplicity.

4.1 Lagrangian duality

There are different methods to obtain an optimal solution of a system, although in some cases those methods need to solve nonlinear equations and inequalities directly, which is better to avoid. The optimization problem can be written as min-max problem as follows

$$\min_{x\epsilon\Omega}\max_{\boldsymbol{\lambda}\geq\mathbf{0}}\mathcal{L}(\boldsymbol{\rho},\boldsymbol{\lambda}) = \min_{\boldsymbol{\rho}\epsilon\Omega}\max_{\boldsymbol{\lambda}\geq\mathbf{0}}\left\{g_0(\boldsymbol{\rho}) + \sum_{i=1}^{l}\lambda_i\cdot g_i(\boldsymbol{\rho})\right\} \tag{25}$$

where $\mathcal{L}$ is the Lagrangian function defined in function of $\boldsymbol{\rho}$, which is the vector that denotes the design variables, and $\boldsymbol{\lambda}$, which is the vector that defines Lagrange multipliers, g_i represents the problem constraints and g_0 is the objective function. Thus, $\mathcal{L}$ is maximized with respect to $\boldsymbol{\lambda}\geq\mathbf{0}$ for a fixed $\boldsymbol{\rho}$, and the result is minimized with respect to $\boldsymbol{\rho}\,\epsilon\,\Omega$, where Ω is the problem domain (Christensen & Klarbring, 2009).

According to Christensen and Klarbring (2009), this problem can be reformulated by an interchanging between min and max in Eq. (25), which results in a completely different problem. However, if the proposed problem is convex and $\boldsymbol{\rho}^*$ is a local minimum, then there exists a $\boldsymbol{\lambda}^*$ that solves the following problem

$$\begin{cases} \max\limits_{\boldsymbol{\lambda}} \varphi(\boldsymbol{\lambda}) \\ \text{subject to: } \boldsymbol{\lambda} \geq \mathbf{0} \end{cases} \tag{26}$$

where the dual objective function $\varphi(\boldsymbol{\lambda})$ is defined as

$$\varphi(\boldsymbol{\lambda}) = \min_{\boldsymbol{x} \epsilon \Omega} \mathcal{L}(\boldsymbol{\rho}, \boldsymbol{\lambda}) \tag{27}$$

and an $\boldsymbol{\rho}^* \epsilon \operatorname{argmin}_{\boldsymbol{\rho}\, \epsilon\, \Omega} \mathcal{L}(\boldsymbol{\rho}, \boldsymbol{\lambda}^*)$ that solves the optimization problem.

4.2 OC Method

A classical approach to solving the problem proposed in Eq. (24) is the OC method. Following the scheme proposed in Christensen and Klarbring (2009), the steps to obtain the design variables are: introducing the following intervening variable

$$y_e = \rho_e^{-\alpha} \tag{28}$$

where α is any number greater than zero. By linearizing the function $c(\boldsymbol{\rho})$ in Eq. (24) and using the intervening variable presented in Eq. (28), so we get

$$c(\boldsymbol{\rho}) \approx c\left(\boldsymbol{\rho^k}\right) + \sum_{e=1}^{N} \left.\frac{\partial c}{\partial y_e}\right|_{\boldsymbol{\rho}=\boldsymbol{\rho^k}} (y_e - y_e^k) \tag{29}$$

where k is the iteration and

$$\frac{\partial c}{\partial y_e} = -\frac{\rho_e^{1+\alpha}}{\alpha} \cdot \frac{\partial c}{\partial \rho_e} \tag{30}$$

where

$$\frac{\partial c}{\partial \rho_e} = -p \cdot (\rho_e)^{p-1} \cdot \boldsymbol{u_e^T} \cdot \boldsymbol{k_e^0} \cdot \boldsymbol{u_e} \tag{31}$$

Since that $\boldsymbol{k_e^0}$ is a positive semidefinite matrix, so this derivative cannot be positive. Inserting Eq. (28) and Eq. (30) in Eq. (29) gives

$$c(\boldsymbol{\rho}) \approx \text{const.} + \sum_{e=1}^{N} b_e^k \cdot \rho_e^{-\alpha} \tag{32}$$

where

$$b_e^k = \frac{p \cdot (\rho_e^k)^{p+\alpha}}{\alpha} \cdot \boldsymbol{u_e^T} \cdot \boldsymbol{k_e^0} \cdot \boldsymbol{u_e} \tag{33}$$

Now, it is possible to reformulate this problem by an approximated subproblem defined as

$$\begin{cases} \min\limits_{\boldsymbol{x}} \sum\limits_{e=1}^{N} b_e^k \cdot \rho_e^{-\alpha} \\ \text{subject to:} \quad \dfrac{V(\boldsymbol{\rho})}{\bar{V}} = f \\ \boldsymbol{K} \cdot \boldsymbol{U} = \boldsymbol{F} \\ \mathbf{0} < \boldsymbol{\rho}_{min} \leq \boldsymbol{\rho} \leq \mathbf{1} \end{cases} \tag{34}$$

The problem presented in Eq. (34) is convex and can be treated by Lagrangian duality, as presented in Section 4.1. Therefore, the Lagrangian function $\mathcal{L}$ is given by

$$\mathcal{L}(\boldsymbol{\rho}, \boldsymbol{\lambda}) = \sum_{e=1}^{N} b_e^k \cdot \rho_e^{-\alpha} + \lambda(V(\boldsymbol{\rho}) - f \cdot \bar{V}) \tag{35}$$

The dual function is

$$\varphi(\lambda) = \min_{\rho_{min} \leq \rho_e \leq 1} \mathcal{L}(\boldsymbol{\rho}, \boldsymbol{\lambda}) = \sum_{e=1}^{N} \min_{\rho_{min} \leq \rho_e \leq 1} [b_e^k \cdot \rho_e^{-\alpha} + \lambda \cdot V(\rho_e)] - \lambda \cdot f \cdot \bar{V} \tag{36}$$

The term to be minimized can be separated and evaluated for each element of the discretized problem.

$$\varphi_e(\rho_e, \lambda) = b_e^k \cdot \rho_e^{-\alpha} + \lambda \cdot V(\rho_e) \tag{37}$$

By minimizing the function in Eq. (37) we get

$$\frac{\partial \varphi_e}{\partial \rho_e} = -\alpha \cdot b_e^k \cdot \rho_e^{(-\alpha-1)} + \lambda \cdot \frac{\partial V}{\partial \rho_e} = 0 \tag{38}$$

From Eq. (38) we find

$$\rho_e = \left(\lambda \cdot \frac{\alpha \cdot b_e^k}{\dfrac{\partial V}{\partial \rho_e}} \right)^{\frac{1}{1+\alpha}} \tag{39}$$

By analyzing the value presented in Eq. (39), the design variable ρ_e can be expressed by the following relation:

$$\rho_e(\lambda) = \begin{cases} \rho_{min} & \text{if } \left(\lambda \cdot \dfrac{\alpha \cdot b_e^k}{\dfrac{\partial V}{\partial \rho_e}}\right)^{\frac{1}{1+\alpha}} < \rho_{min} \\ \left(\lambda \cdot \dfrac{\alpha \cdot b_e^k}{\dfrac{\partial V}{\partial \rho_e}}\right)^{\frac{1}{1+\alpha}} & \text{if } \rho_{min} < \left(\lambda \cdot \dfrac{\alpha \cdot b_e^k}{\dfrac{\partial V}{\partial \rho_e}}\right)^{\frac{1}{1+\alpha}} < 1 \\ 1 & \text{if } \left(\lambda \cdot \dfrac{\alpha \cdot b_e^k}{\dfrac{\partial V}{\partial \rho_e}}\right)^{\frac{1}{1+\alpha}} > 1 \end{cases} \tag{40}$$

The solution of the problem presented in Eq. (34) is given by inserting the value of λ^* into Eq. (40) and the next iteration of the method is going to be

$$\rho_e^{k+1} = \rho_e(\lambda^*) \tag{41}$$

As the number α appears only in the form, so it can be introduced the following notation:

$$\eta = \frac{1}{1+\alpha} \tag{42}$$

which is a numerical damping factor taken as $1/2$. Finally, the step iteration can be described as

$$\rho_e^{k+1} = \min\left\{\max\left[\left(\lambda \cdot \frac{p \cdot \boldsymbol{u_e^T} \cdot \boldsymbol{K} \cdot \boldsymbol{u_e}}{\dfrac{\partial V}{\partial \rho_e}} \cdot (\rho_e^k)^{(p+\alpha)}\right)^{\eta}, \rho_{min}\right], 1\right\} \tag{43}$$

4.3 Penalization of intermediate values

According to Sigmund and Petersson (1998), one of the reasons to use penalization techniques to penalize intermediate densities is the post-processing of solutions to relaxed problems. For example, in manufacturing cases when the objective is to get a homogenized topology, then the penalization is performed to exclude intermediate density regions and to have a more macroscopic 0-1 solutions.

In solid isotropic materials, the intermediate designs are penalized through the Young modulus by using the following constitutive matrix for plane stress state:

$$\boldsymbol{D} = \frac{\rho_e^p \cdot E}{1-\nu^2} \cdot \begin{bmatrix} 1 & \nu & 0 \\ \nu & 1 & 0 \\ 0 & 0 & \dfrac{1-\nu}{2} \end{bmatrix} \tag{44}$$

Then, the "effective" Young modulus is given by $\rho_e^p \cdot E$.

5 NUMERICAL RESULTS

Two examples are analyzed in this section, comparing the optimized topologies obtained by the Finite Volume Theory (FVT) with those ones based on the finite element method analysis, employing the Q4 and Q8 elements. Besides, numerical aspects are investigated, such as number of iterations, processing time and the convergence. The proposed convergence analysis is based on the difference between the topologies obtained by the coarse meshes with that one from the finest mesh. In this sense, it was necessary to define the following error measure:

$$\text{Error} = \frac{\int_{\text{V}} |\rho - \rho_{ref}| \text{dV}}{\int_{\text{V}} \rho_{ref} \text{dV}} \tag{45}$$

where ρ is the material relative density function of the current mesh, and ρ_{ref} is the material relative density function obtained by the finest mesh.

With the goal to have a fair comparison and to show the numerical issues of the gradient-based optimization algorithms, the following results were obtained without filters, in other words, without image processing.

In order to avoid the local minima issue, the continuation scheme has been adopted, where a gradually increase of the density penalty factor p is employed during the process, assuming the values 1, 2 and 2.9, which ensures the convexity of the process, avoiding a local minima and gradually converging to the desired 0-1 design.

The adopted convergence criterion is based on the maximum difference between the material relative density functions obtained by successive steps, in this way, the looping finishes when:

$$\max\left(|\boldsymbol{\rho}^{k+1} - \boldsymbol{\rho}^{k}|\right) \leq \text{TOLERANCE} \tag{46}$$

where $\boldsymbol{\rho}^{k}$ is the material relative density vector of the previous step, and $\boldsymbol{\rho}^{k+1}$ is the material relative density vector of the current step. The following values were adopted for the numerical parameters: $\text{TOLERANCE} = 0.01$ and $\rho_{min} = 0.001$. The computational environment, in terms of programming language and machine, can be specified as follows: MatLab R2013b (64-bits)/Intel® Core™ i3 CPU 2.93 GHz/4.0 GB RAM/64-bits.

5.1 *Michell* structure

The *Michell* structure is shown in Figure 2, where the following values are adopted for the geometric and physical parameters: $L = 800\,mm$, $H = 400\,mm$, $t = 10\,mm$ (thickness), $E = 10^{-6}\ N/mm^2$, $\nu = 0.3$ and $P = 1\,N$. Taking advantage of the symmetry, just half part of the design domain was analyzed, employing boundary conditions that reflect this symmetry.

As can be noticed in Figure 3, the checkerboard pattern is really an issue for the optimized topologies obtained by the finite-element analysis employing the Q4 element, even for the finest mesh. This problem does not occur for the optimized topologies based on the analysis employing the Q8 element and the finite volume theory. The result obtained by the coarsest

mesh shown in Figure 3, based on the finite volume theory, already gives a good idea of the optimized topology.

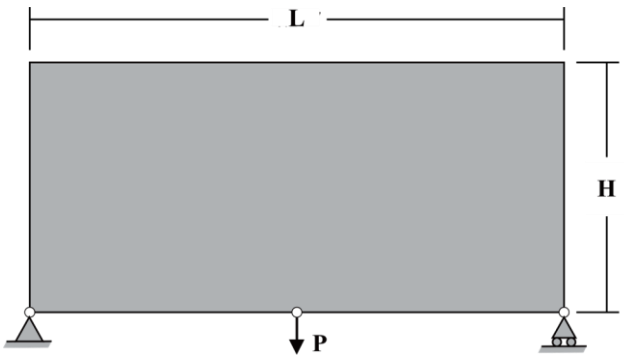

Figure 2. *Michell* structure.

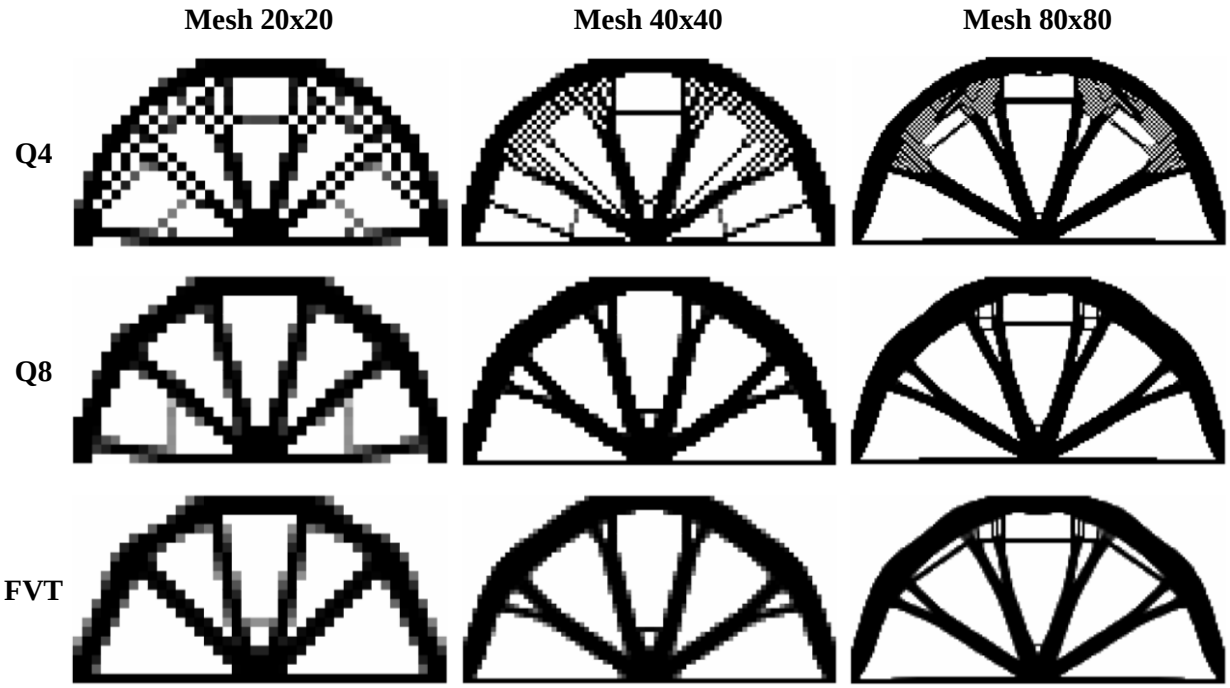

Figure 3. Optimized topologies of the *Michell* structure.

The Table 2 shows that the number of iterations does not change much from one approach to another. In other hand, the processing time does change from one approach to another, for instance, the processing time of the gradient-based optimization algorithm based on the finite-element analysis employing the Q8 element, for the finest mesh, is 3.5 times higher than the same analysis employing the finite volume theory. The same analysis employing the Q4 element is 2.8 faster than the analysis employing the finite volume theory. The Number of Degrees Of Freedom (NDOF) explains partially those differences in the processing time, because it defines the size of the global system of equations. In terms of convergence, based on the comparison with the optimized topologies obtained by the finest mesh, the analysis employing the Q8 element has practically the same efficiency of the analysis based on the finite volume theory. The same cannot be said for the analysis employing the Q4 element, clearly less efficient, in addition to the checkerboard-problem.

Proceedings of the XXXVIII Iberian Latin-American Congress on Computational Methods in Engineering P.O. Faria, R.H. Lopez, L.F.F. Miguel, W.J.S. Gomes, M. Noronha (Editores), ABMEC, Florianópolis, SC, Brazil, November 5-8, 2017.

Table 2. Convergence study of the *Michell* structure.

Analysis	Mesh	NDOF	Error (%)	Number of Iterations:				Processing Time (sec)			
				p=1	p=2	p=2.9	Total	p=1	p=2	p=2.9	Total
Q4	10x10	242	100.96	10	61	21	92	0.13	0.49	0.18	0.8
	20x20	882	64.88	16	70	24	110	1.00	2.55	0.86	4.41
	40x40	3362	42.48	25	88	25	138	7.83	23.97	6.50	38.3
	80x80	13122	0.00	33	76	32	141	199.12	395.88	149.88	744.88
Q8	10x10	682	73.86	8	74	17	99	0.18	1.85	0.43	2.46
	20x20	2562	53.39	13	69	27	109	1.99	10.42	3.99	16.4
	40x40	9922	25.42	22	66	19	107	51.77	150.57	42.68	245.02
	80x80	39042	0.00	32	146	16	194	1244.10	5549.17	607.61	7400.88
FVT	10x10	440	73.97	10	46	60	116	0.27	1.00	0.81	2.08
	20x20	1680	58.20	15	60	58	133	0.95	4.28	4.10	9.33
	40x40	6560	26.33	23	89	41	153	13.53	52.18	24.61	90.32
	80x80	25920	0.00	32	96	59	187	354.02	1074.71	664.10	2092.83

5.2 *Messerschmitt–Bölkow–Blom* (MBB) beam

The *Messerschmitt–Bölkow–Blom* (MBB) beam is shown in Figure 4, where the following values are adopted for the geometric and physical parameters: $L = 12\,m$, $H = 2\,m$, $t = 0.01\,m$ (thickness), $E = 2.10^{11}\ N/m^2$, $\nu = 0.3$ and $P = 200\,N$. Taking advantage of the symmetry, just half part of the design domain was analyzed, employing boundary conditions that reflect this symmetry.

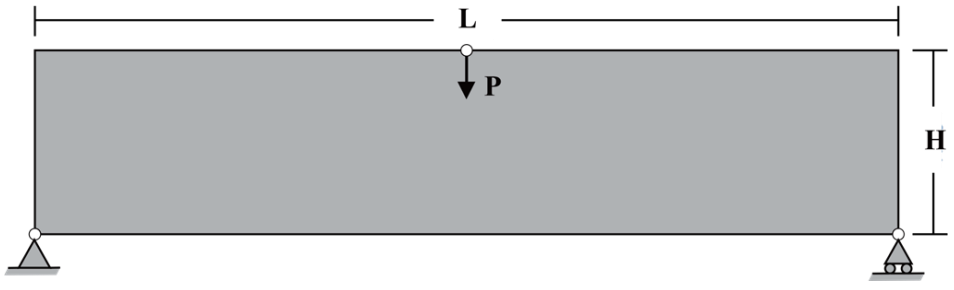

Figure 4. *Messerschmitt–Bölkow–Blom* (MBB) beam.

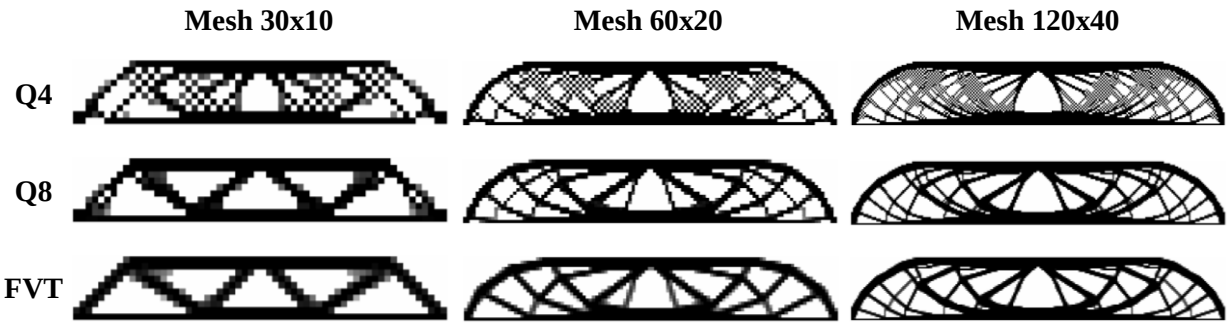

Figure 5. Optimized topologies of the *Messerschmitt–Bölkow–Blom* (MBB) beam.

Table 3. Convergence study of the *Messerschmitt–Bölkow–Blom* (MBB) beam.

Analysis	Mesh	NDOF	Error (%)	Number of Iterations:				Processing Time (sec)			
				p=1	p=2	p=2.9	Total	p=1	p=2	p=2.9	Total
Q4	15x5	192	67.85	9	24	28	61	0.10	0.20	0.24	0.54
	30x10	682	63.18	14	55	15	84	0.32	1.74	0.34	2.4
	60x20	2562	54.13	19	94	38	151	3.36	15.33	5.96	24.65
	120x40	9922	0.00	30	140	51	221	92.67	386.69	134.06	613.42
Q8	15x5	532	65.70	8	33	51	92	0.24	0.64	0.97	1.85
	30x10	1962	58.10	11	73	18	102	1.05	7.06	1.60	9.71
	60x20	7522	55.90	17	148	42	207	20.88	173.88	48.23	242.99
	120x40	29442	0.00	28	106	45	179	609.55	2261.96	940.97	3812.48
FVT	15x5	340	67.02	8	8	53	69	0.16	0.13	0.93	1.22
	30x10	1280	59.79	10	83	53	146	0.34	3.52	1.71	5.57
	60x20	4960	51.56	18	93	56	167	6.37	32.96	19.78	59.11
	120x40	19520	0.00	27	96	65	188	176.11	538.49	346.66	1061.26

As the previous example, analyzing the Figure 5, the checkerboard pattern is really an issue for the optimized topologies obtained by the finite-element analysis employing the Q4 element, even for the finest mesh. This cannot be said for the optimized topologies based on the analysis employing the Q8 element and the finite volume theory. However, we can see this problem very localized for the coarsest mesh employing the Q8 element, which disappears for the second mesh shown in Figure 5. The checkerboard pattern is definitely not an issue for the analysis based on the finite volume theory.

Once again, the Table 3 shows that the number of iterations does not change much from one approach to another. In other hand, the same cannot be said for the processing time, for instance, the processing time of the analysis based on the finite-element method employing the Q8 element, for the finest mesh, is 3.6 times higher than the same analysis employing the finite volume theory. The same analysis employing the Q4 element is 1.7 faster than the analysis

employing the finite volume theory. As before, the Number of Degrees Of Freedom (NDOF) can explain those differences in the processing time, because it defines the size of the global system of equations. In terms of convergence, based on the comparison with the optimized topologies obtained by the finest mesh, the analyses employing different approaches have demonstrated practically the same efficiency.

6 CONCLUSIONS

The gradient-based optimization algorithm employing the finite volume theory demonstrated to be very efficient for the analyzed examples, in comparison with the same technique based on the finite-element method, in addition of the absence of some numerical issues, as the checkerboard pattern. The checkerboard pattern is definitely an issue for the optimized topologies obtained by the Q4 element, and can occur very locally for the Q8 element.

The use of image processing was avoided, with the goal to have a fair and transparent comparison between the different approaches, besides, the analysis without image processing allows the verification of the numerical issues, especially the checkerboard pattern. The continuation scheme was adopted, where a gradually increase of the density penalty factor p is employed during the process, which ensures the convexity of the process, avoiding a local minima and gradually converging to the desired 0-1 design.

Based on these results, we can justify a continuation of this investigation, exploring different aspects of the finite volume theory that guarantee fast convergence and numerical stability, such the satisfaction of the equilibrium equations locally at the subvolume level and the static and kinematic compatibilities, in an average sense, between different subvolumes along the shared faces.

ACKNOWLEDGMENTS

The authors acknowledge the financial support provided by the Brazilian federal agency CNPq.

REFERENCES

Arora, J., 2004. *Introduction to Optimum Design*. Elsevier Academic Press.

Bendsøe, M. P., 1989. Optimal shape design as a material distribution problem. *Structural Optimization*, 1, 193-202.

Bendsøe, M. P. and Kikuchi, N., 1988. Generating Optimal Topologies in Structural Design using a Homogenization Method. *Computer Methods in Applied Mechanics and Engineering*, 71, 197-224.

Bendsøe, M. P. and Sigmund, O., 2004. *Topology Optimization: Theory, Methods and Applications*. Springer, New York.

Cavalcante, M. A. A., Marques, S. P. C. and Pindera, M.-J. , 2007a. Parametric formulation of the finite volume theory for functionally graded materials. Part I: Analysis. *Journal of Applied Mechanics*, 74 (5), 935-945.

Cavalcante, M. A. A., Marques, S. P. C. and Pindera, M.-J., 2007b. Parametric formulation of the finite volume theory for functionally graded materials. Part II: Numerical Results. *Journal of Applied Mechanics*, 74 (5), 946-957.

Cavalcante, M. A. A., Marques, S. P. C. and Pindera, M.-J., 2008. Computational aspects of the parametric finite volume theory for functionally graded materials. *Journal of Computational Materials Science*, 44 (2), 422-438.

Cavalcante, M. A. A. and Pindera, M.-J., 2012a. Generalized finite volume theory for elastic stress analysis in solid mechanics. Part I: framework. *Journal of Applied Mechanics*, 79, 051006-1.

Cavalcante, M. A. A. and Pindera, M.-J., 2012b. Generalized finite volume theory for elastic stress analysis in solid mechanics. Part II: Results. *Journal of Applied Mechanics*, 79, 051007-1.

Christensen, P. and Klarbring, A., 2009. *An Introduction to Structural Optimization*. Springer Science.

Coutinho, K., 2006. *Método de Otimização Topológica em Estruturas Tridimensionais*. Master thesis, Universidade Federal do Rio Grande do Norte.

Eschenauer, H. A. and Olhoff, N., 2001. *Topology Optimization of Continuum Structures: A Review*. *Applied Mechanics Review*, 54, 331-390.

Johnsen, S., 2013. *Structural Topology Optimization: Basic Theory, Methods and Applications*. Master Thesis, Norwegian University of Science and Technology.

Mlejnek, H. P., 1992. Some aspects of the genesis of structures. *Structural Optimization*, 5, 64-69.

Petersson, J. and Sigmund, O., 1998. Slope constrained topology optimization. *International Journal* for *Numerical Methods* in *Engineering*, 41, 1417–1434.

Rouhi, M., 2009. *Topology optimization of continuum structures using element exchange method*. MS Thesis, Mississippi State University.

Sigmund, O., 2001. A 99 line topology optimization code written in Matlab. *Structural and Multidisciplinary Optimization*, vol. 21, pp. 120-127.

Sigmund, O. and Petersson, J., 1998. Numerical instabilities in topology optimization: A survey on procedures dealing with checkerboards, mesh-dependencies and local minima. *Structural Optimization*, 16 (1), 68-75.

Stolpe, M. and Svanberg, K., 2001a. On the trajectories of penalization methods for topology optimization. *Structural and Multidisciplinary Optimization*, 21, 128–139.

Stolpe, M. and Svanberg, K., 2001b. An alternative interpolation scheme for minimum compliance topology optimization. *Structural and Multidisciplinary Optimization*, 22, 116-124.

Zhou, M. and Rozvany, G. I. N., 1991. The COC algorithm, part II: Topological, geometry and generalized shape optimization. *Computer Methods in Applied Mechanics and Engineering*, 89, 197-224.

APPENDIX

Auxiliary matrices employed in the Finite Volume Theory:

$$\boldsymbol{A}_{(8\times8)}^{(q)} = \begin{bmatrix} 0 & -\frac{1}{2}h_q & 0 & \frac{1}{4}h_q^2 & 0 & 0 & 0 & 0 \\ 0 & 0 & 0 & 0 & 0 & -\frac{1}{2}h_q & 0 & \frac{1}{4}h_q^2 \\ \frac{1}{2}b_q & 0 & \frac{1}{4}b_q^2 & 0 & 0 & 0 & 0 & 0 \\ 0 & 0 & 0 & 0 & \frac{1}{2}b_q & 0 & \frac{1}{4}b_q^2 & 0 \\ 0 & \frac{1}{2}h_q & 0 & \frac{1}{4}h_q^2 & 0 & 0 & 0 & 0 \\ 0 & 0 & 0 & 0 & 0 & \frac{1}{2}h_q & 0 & \frac{1}{4}h_q^2 \\ -\frac{1}{2}b_q & 0 & \frac{1}{4}b_q^2 & 0 & 0 & 0 & 0 & 0 \\ 0 & 0 & 0 & 0 & -\frac{1}{2}b_q & 0 & \frac{1}{4}b^2 & 0 \end{bmatrix} \tag{A.1}$$

$$\boldsymbol{a}_{(8\times2)}^{(q)} = \begin{bmatrix} 1 & 0 \\ 0 & 1 \\ 1 & 0 \\ 0 & 1 \\ 1 & 0 \\ 0 & 1 \\ 1 & 0 \\ 0 & 1 \end{bmatrix} \tag{A.2}$$

$$\boldsymbol{B}_{(8\times8)}^{(q)} = \begin{bmatrix} 0 & -C_{44}^{(q)} & 0 & \frac{3}{2}h_q C_{44}^{(q)} & -C_{44}^{(q)} & 0 & 0 & 0 \\ -C_{23}^{(q)} & 0 & 0 & 0 & 0 & -C_{22}^{(q)} & 0 & \frac{3}{2}h_q C_{22}^{(q)} \\ C_{22}^{(q)} & 0 & \frac{3}{2}b_q C_{22}^{(q)} & 0 & 0 & C_{23}^{(q)} & 0 & 0 \\ 0 & C_{44}^{(q)} & 0 & 0 & C_{44}^{(q)} & 0 & \frac{3}{2}b_q C_{44}^{(q)} & 0 \\ 0 & C_{44}^{(q)} & 0 & \frac{3}{2}h_q C_{44}^{(q)} & C_{44}^{(q)} & 0 & 0 & 0 \\ C_{23}^{(q)} & 0 & 0 & 0 & 0 & C_{22}^{(q)} & 0 & \frac{3}{2}h_q C_{22}^{(q)} \\ -C_{22}^{(q)} & 0 & \frac{3}{2}b_q C_{22}^{(q)} & 0 & 0 & C_{23}^{(q)} & 0 & 0 \\ 0 & -C_{44}^{(q)} & 0 & 0 & -C_{44}^{(q)} & 0 & \frac{3}{2}b_q C_{44}^{(q)} & 0 \end{bmatrix} \tag{A.3}$$

where $C_{ij}^{(q)}$ are the components of the material stiffness matrix.